JOURNAL OF PROPULSION AND POWER
Vol. 16, No. 6, November–December 2000

Performance of Evaporative Cycle Gas Turbines Derived from Aeroengines

Sergio Mario Camporeale*
Università di Reggio Calabria, 89100 Reggio Calabria, Italy
and
Bernardo Fortunato†
Politecnico di Bari, 70125 Bari, Italy

The modification of the thermodynamic cycle could be an attractive opportunity for improving the performance of aeroderivative gas turbines. The simulation of a aeroderivative gas turbine modified to realize a nonintercooled regenerative water-injected (RWI) cycle is presented. The thermodynamic analysis of the RWI cycle shows that aeroderivative gas turbines with a pressure ratio from 16 to 20 can reach thermal efficiency of 45%. The design of the enhanced gas turbine is carried out under the hypotheses that the compressor is unchanged and that the stator vanes of the two-stage high-pressure turbine are partially opened to accommodate to the larger mass flow produced by water injection. The other characteristics of the turbine stator blades (internal and external area and internal coolant passages) and the rotor blades are supposed unchanged. A stage-by-stage off-design model, including blade cooling and hydrodynamics, is introduced for predicting the performance of the modified high-pressure turbine. The effects produced by modification of the cycle are then evaluated. The off-design incidence angles at the rotor inlet of both the stages appear to limit the maximum amount of the water that can be injected per air mass unit. The increase of the blade temperature instead can be compensated by decreasing the turbine inlet temperature or by refrigerating the cooling air. The mathematical model adopted for simulating the on-design and the off-design behavior of the enhanced gas turbine is described.

Nomenclature

C, W, U	=	absolute, relative, peripheral velocity
c_p	=	specific heat at constant pressure
h	=	heat transfer coefficient
i	=	enthalpy for gas and superheated vapor
$\hat{\imath}$	=	enthalpy for liquid water
K	=	orifice coefficient, defined by Eq. (A19)
k	=	specific heat ratio
M	=	Mach number
MW	=	molecular weight
$\dot{m}$	=	mass flow rate
$\dot{m}_{\mathrm{cl}}$	=	coolant mass flow rate per row
P	=	power
Pr	=	Prandtl number
p	=	pressure
Re	=	Reynolds number
St	=	Stanton number
s	=	entropy
T	=	temperature
w	=	specific work
x_w	=	water-to-air ratio, defined by Eq. (3)
Y	=	cooling air mixing momentum loss parameter
α_2, α_3	=	absolute velocity angle, measured from the axial direction
β	=	compressor pressure ratio
Γ	=	mass flow parameter, defined by Eq. (8)
ΔT	=	temperature variation
$\Delta\theta$	=	incidence angle
ε	=	heat transfer efficiency
η	=	efficiency
Θ	=	dimensionless temperature
ρ	=	density
Φ	=	blade cooling effectiveness, $(T_g - T_b)/(T_g - T_{\mathrm{cl}})$
φ	=	flow coefficient
Ψ	=	stage load coefficient

Subscripts

b	=	blade
cl	=	coolant
e	=	external, gas side
g	=	gas
i	=	internal, coolant side
in, out	=	inlet, outlet
is	=	isentropic
rot	=	turbine rotor row
st	=	turbine stator row
t	=	turbine stage
w	=	water

Superscripts

0	=	stagnation value
$\prime$	=	partial (referred to the pressure)
*	=	design point of the base aeroderivative gas turbine

I. Introduction

IN the last several years the performance of the aeroderivative gas turbines has been significantly increased. The use of advanced fluid dynamics computational methods has improved the efficiency of the compressor and of the turbine. New materials for the turbine blades and improved effectiveness of the cooling systems have offered the possibility to increase the turbine inlet temperature and, consequently, the cycle efficiency and specific work. Further, performance improvement can be obtained with modification of the thermodynamic cycle. For small and middle power plants ranging

Received 26 March 1997; revision received 27 October 1999; accepted for publication 8 November 1999.

*Assistant Professor, Dipartimento di Meccanice Materiali, via Graziella, Contrada Feo di Vito; camporea@ing.unirc.it.

†Full Professor, Istituto di Macchine ed Energetica, via Re David 200; fortunat@imebf.poliba.it. Member AIAA.

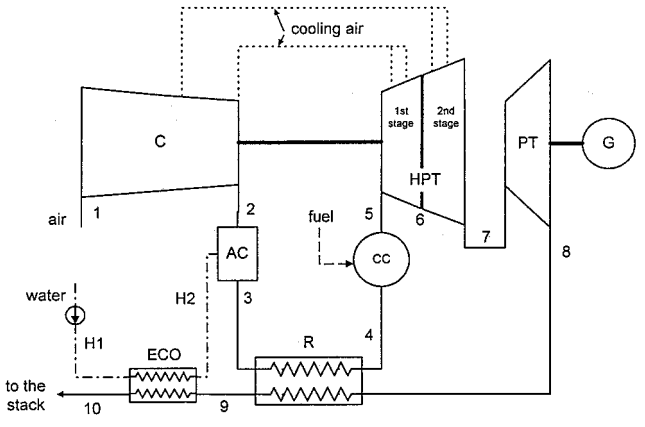

Fig. 1 Plant arrangement of the RWI cycle aeroderivative gas turbine.

within 20–30 MW, evaporative cycles may be an alternative to combined cycles because they allow an increase of efficiency and specific work without a bottoming steam turbine.

A mathematical model is offerred for the simulation of the on-design and off-design performance of the air cooled turbine used in evaporative cycles (Appendix A). The applications of this model are to analyze the effects of the modifications of the cycle on the behavior of the gas turbine, to do a part-load analysis, and to analyze the performance of the power plant at various ambient temperatures.

This paper deals with the upgrade of a gas turbine composed of a single shaft gas generator and a power turbine. The single shaft arrangement suggests consideration of an upgrade to non-intercooled cycles because insertion of the intercooling requires modification of the compressor.

The plant arrangement of the regenerative water-injected (RWI) cycle is shown in Fig. 1. Water is injected into the airstream in an aftercooler (AC) placed at the compressor discharge. The air–water mixture is then heated in a regenerative heat exchanger (R) before entering in the combustion chamber (CC). The water, before being injected in the aftercooler, is heated by the hot gas leaving the regenerator in a heat exchanger called an economizer (ECO).

The addition of water to the air increases the turbine mass flow and power output while the power absorbed by the compressor remains about constant. With respect to a simple regenerative cycle, the air–vapor mixture enters the heat exchanger at a lower temperature. This allows the increase of heat recovery and the reduction of the gas temperature in the exhaust stack, with a favorable effect on the cycle efficiency.

The thermodynamic analysis of this cycle has been given by various authors. Gasparovich and Hellemans[1] discussed the cycle performance under the simplified hypotheses of constant heat capacity of the working fluids. El-Masri[2] investigated the RWI cycle modified with intercooling and water injection in the regenerator. Annerwall and Svedberg[3] compared the RWI cycle with other evaporative and steam-injected cycles at constant pressure ratio (13.5) without providing information on the effects of blade cooling. Chiesa et al.[4] provide the thermodynamic analysis of the RWI cycle with intercooling for an aeroderivative gas turbine with pressure ratio of 30. Horlock[5] examined a cycle, which he called "Evaporative Gas Turbine cycle," with and without intercooling, taking into account, in a simplified manner, the effects of turbine cooling.

In Ref. 6, the authors have taken into account the variation of the thermodynamic properties of the working fluids due to water injection. In Ref. 5, Horlock has taken into account the effects of the turbine cooling with a simplified approach for the evaluation of the coolant mass flow. From Ref. 5, it appears that for the RWI cycle the efficiency peaks to 50% at a relatively low pressure ratio ($\beta = 8$) but little decrement is observed by increasing the pressure ratio up to the maximum value considered in his calculations ($\beta = 16$).

The RWI cycle with intercooling has been analyzed by various authors.[2–5,7] In Ref. 5, the RWI cycle with and without intercooling are compared one to each other. It appears that intercooling provides little benefit to the plant thermal efficiency (about 1%). The main effect of intercooling is a significant decrease of the amount of water injected.

Results provided in Ref. 5 confirm the interest of a deeper investigation about the possibility of upgrading the aeroderivative gas turbine in a RWI cycle. The interest in aeroderivative gas turbines for the RWI cycle power plants comes from the following considerations:

1) A new gas-turbine engine specifically designed for a mixed gas/steam cycle does not seem to be economically feasible because of the costs required to design and produce a completely new engine.

2) The enhanced power plant can be obtained with the substitution of the power turbine and a limited number of modifications of the gas generator [compressor and high-pressure turbine (HPT)].

A conventional thermodynamic analysis is not able to predict the performance of a power plant obtained by upgrading an aeroderivative gas turbine. The insertion of evaporative units produces different effects than a simple dry regeneration. The injection of water or steam and the insertion of heat exchangers modify the gas generator operating region and the enthalpic drop in the power turbine. The mechanical energy balance of the shaft connecting the compressor and the HPT is altered by the increase of mass flow expanding in the turbine. Opening the HPT nozzle vanes is generally needed to avoid the decrease of turbine inlet temperature.

Modification of the secondary cooling system is also needed. The cooling air can no longer be extracted from the plenum outside the combustion chamber because the temperature of the air entering the combustion chamber is increased by regeneration. A complete, new design of the blade cooling system can be avoided by the modification of the secondary air cooling circuit for extracting the air directly from the compressor. Moreover, the refrigeration of the cooling air is also considered for increasing the turbine inlet temperature.

The performance of the upgraded system can be predicted by means of an off-design analysis of the core engine in the modified plant configuration.[6,8,9] For this reason, a mathematical model able to predict the performance of the upgraded aeroderivative gas turbine is introduced. For a better prediction of the turbine expansion, the mathematical model includes a stage-by-stage off-design analysis for the turbine and the simulation of the air cooling off-design behavior. This model provides a suitable evaluation of the temperature for the blades and for the exhaust gas exiting the turbine.

II. Characteristics of the Base Aeroderivative Engine

The enhanced gas turbine is supposed to originate from an aeroderivative gas turbine, composed of a gas generator and a power turbine. The gas generator includes a multistage axial compressor, a combustion chamber, and an HPT.

Knowledge of the engine characteristics is needed to evaluate the off-design behavior of the gas turbine. Generally these data are manufacturers' proprietary information and not available for publication. Therefore, a preliminary design of the base engine has been carried out to obtain the parameters needed for the off-design analysis.

The General Electric Company LM2500 is a typical aeroderivative gas turbine considered as the reference engine.[10,11] A limited set of information is available from the technical reports from the manufacturer[10,11] and from the literature.[12] Such data are about the longitudinal section of the engine (lacking dimensions), the compressor characteristic map,[10] and the global performance of the up-to-date version of the engine.[11] Some dimensional information (such as the hub-to tip ratio) can be obtained from the longitudinal section of the engine. Other data, such as the turbine inlet temperature, are collected from the technical literature concerning up-to-date aeroderivative gas turbines.[3,4,7]

The set of data used in the calculations of this section are summarized in Table 1. Such assumptions resulted from a trial and error procedure carried out to reproduce as much as possible the dimensional characteristics and the global performance of the real engine.

The HPT is composed of two cooled stages. The maximum blade temperature is assumed to be 1100 K for the first-stage stator row and 1000 K for second-stage stator row and for both the rotor rows.

Table 1 Basic assumptions for the design of the base gas turbine and the thermodynamic analysis of the RWI cycle

Location	Parameter
Compressor	Polytropic efficiency 0.915
Combustion chamber	Pressure losses $\Delta p/p = 4\%$, combustion efficiency 0.996
Fuel	Methane, 50.0 MJ/kg LHV
HPT first stage	$\Psi = 1.5$, $\phi = 0.5$, $\alpha_3 = 0$ deg, $\eta_t = 0.9$, $T_{b,\mathrm{st}} = 1100$ K, $T_{b,\mathrm{rot}} = 1000$ K, $St_e = 0.005$, $A_e/A_g = 4$, $Y_{\mathrm{st}} = 0.5$, $Y_{\mathrm{rot}} = 0.5$ cooling system internal and film cooling, $\varepsilon = 0.5$; $\eta_{f\mathrm{ad}} = 0.15$ (both for stator and rotor rows)
HPT second stage	See first stage, except $T_{b,\mathrm{st}} = 1000$ K, cooling system, internal cooling $\varepsilon = 0.5$ (both for stator and rotor rows)
PT	Polytropic efficiency 0.915, diffuser recovery = 50% of the exit kinetic head
Friction and accessory loss	0.5% of the turbomachine work
Electric generator loss	2% of the shaft power

Table 2 Predicted performance of the aeroderivative gas turbine compared with data extracted from Ref. 11

Parameter	Predicted performance	Performance from Ref. 11
Shaft power, MW	23.25	23.3
Exhaust gas flow, kg/s	68.7	68.9
LHV efficiency, %	37.6	37.5
Exhaust temperature, K	795.1	796

Blades are considered cooled by means of internal convection cooling and film cooling. For the first-stage blades, the cooling air is extracted from the compressor outlet. For the second-stage blades, the cooling air is extracted from an intermediate section of the multistage compressor.

The results of the design procedure are given in Appendix B. The global performance, the cycle state points, and the HPT characteristics are given therein. Note that the HPT is close to the choking because the Mach number at the stator row exit is about 0.9 for both the stages. The hub-to-tip ratio for the first stage is rather low, but not too far from the value that can be obtained from scale measurements on the longitudinal section of the real engine. The rotational speed (9655 rpm) is almost equal to the value given in Ref. 12. The cooling effectiveness resulted from calculations for each row of the HPT appears to be in agreement with data reported in Ref. 13.

In Table 2, the global performance obtained from the described design procedure are compared with the results given in Ref. 10. The performance given by the manufacturer is obtained with no inlet/exhaust losses and no heat losses. Taking into account the preceding consideration and the simplified approach adopted for calculations, the agreement seems to be good, and the design of the engine seems to be sufficiently sound and similar to the real engine for the purpose of this work.

III. Thermodynamic Analysis of the RWI Cycle

A. Description of the RWI Cycle

The RWI cycle is plotted in Fig. 2 on a temperature–entropy diagram. In this diagram, the entropy of the mixtures is evaluated using total pressure instead of the partial pressure of each component,[2] neglecting the change in the quantity of the gas working fluids due to air extraction for cooling and water injection for cycle enhancement. In the analysis of the cycle it is necessary to take into account the modification of the thermodynamic properties of the working fluids caused by the variation of the temperature and the chemical composition due to water injection, combustion, and mixing with cooling air.

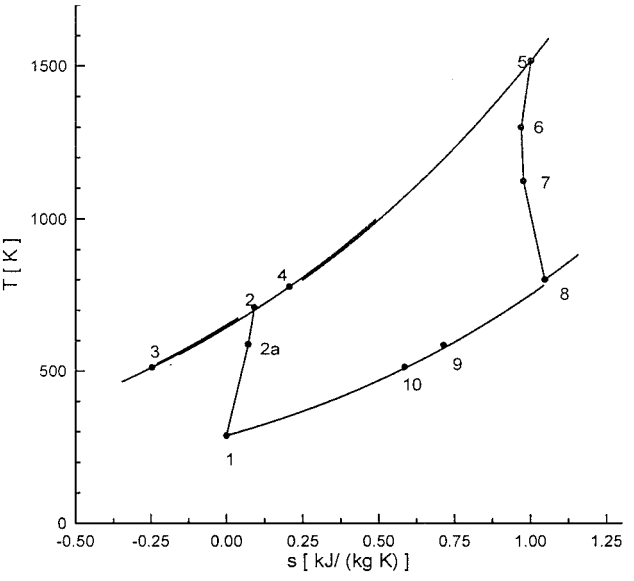

Fig. 2 Thermodynamic diagram of the RWI cycle.

From the aftercooler outlet to the combustion chamber inlet, the flow can be considered as a mixture of two components: air and steam produced by evaporation of the water injected. The total mass flow rate is given by

$$\dot{m} = \dot{m}_a + \dot{m}_w \tag{1}$$

where $\dot{m}_a$ has the same composition and water content of the ambient air, and $\dot{m}_w$ is the water injected mass flow.

After being discharged by the combustion chamber, the flow can be considered as a mixture composed by stoichiometric combustion products, dilution air, and steam. The total mass flow is given by

$$\dot{m} = \dot{m}_g + \dot{m}_w \tag{2}$$

where $\dot{m}_g$ is the sum of the stoichiometric combustion products and the dilution air and $\dot{m}_w$ is the injected water that flows through the combustion chamber.

The thermodynamic properties are evaluated on the basis of the chemical composition of the mixtures. The specific heat coefficients and the enthalpy of the chemical species (except steam) are considered to vary only with temperature; the values of specific heat and enthalpy are obtained using a polynomial fit to the thermodynamic data against the temperature.[14]

The properties of superheated steam are considered to vary with temperature and partial pressure.[15] The partial pressures of air and steam are considered for calculations in the mixer to evaluate the thermodynamic properties of the mixture and to detect the saturation conditions.

To allow a comparison with the performance of the base aeroderivative gas turbine, the assumptions for the simulation of the RWI cycle are the same as adopted for the design of the base engine and listed in Table 1. The thermodynamic analysis has been carried out under the hypothesis that the blade cooling parameters are constant. The air cooling flow rates are supposed to vary as much as needed to keep constant the temperature of the blades.

For the evaluation of the heat recovered in the R and in the ECO, a minimum temperature difference $\Delta T_{\min}$ is assumed between the hot and the cold fluid. To avoid the vaporization in the ECO, the feed water is pumped to a pressure higher than the saturation pressure corresponding to maximum temperature in the ECO. Parameters regarding the AC and the heat exchangers are listed in Table 3.

To identify the amount of the water injected independently from the amount of the air extracted from the compressor for turbine blade cooling, the following parameter is introduced:

$$x_w = \dot{m}_w/\dot{m}_{a,1} \tag{3}$$

where $\dot{m}_w$ is the amount of the water injected in the AC and $\dot{m}_{a,1}$ is the air mass flow rate at the compressor inlet.

B. Effects of the Amount of Water Injected

The cycle performance obtained increasing the amount of the water injected is first evaluated assuming $\beta = 18.7$ and turbine inlet temperature (TIT) = 1523 K. The specific enthalpy (per mass unit) for gas and superheated vapor are indicated by i and the specific water (liquid) enthalpy by $\hat{i}$. The number indicated as subscript refer to the cycle points in Figs. 1 and 2. As β and TIT are assumed to be constant, points 2 and 5 in the cycle of Fig. 1 are constant and independent x_w. The increase of water injected results in the decrease of the temperature T_3 at the AC exit. The temperature T_8 of the gas exiting the power turbine can be assumed almost constant, although water injection affects the specific heat ratio in the expansion and the amount of the cooling air.

In the AC, the evaporation of the water injected is caused by the combined effects of 1) water flashing in the AC in which the partial pressure of water vapor is much lower than the pressure of the entering water and 2) heat extraction from the compressed air.

Referring to the cycle state points of Fig. 2, the steady flow energy equation for the AC

$$\dot{m}_w(i_{w,3} - \hat{i}_{w,H2}) = \dot{m}_{a,3}(i_{a,2} - i_{a,3}) \tag{4}$$

allows the evaluation of the temperature T_3 of the air–vapor mixture leaving the AC. Figure 3a shows the decrease of T_3 caused by the increase of the amount of water injected. In the evaluation of T_3, the reduction of $\dot{m}_{a,3}$ due to the increase of the cooling air extracted from the compressor is taken into account.

Table 3 Additional assumptions for the aftercooler and the heat exchangers

Location	Parameter
AC	Pressure loss $\Delta p/p$ = 3%
R	Pressure loss $\Delta p/p$ = 2% (both air and gas side)
	$\Delta T_{\min}$ (pinch point) = 30 K
ECO	Pressure loss $\Delta p/p$ = 1% (gas side)
	$\Delta T_{\min}$ (pinch point) = 20 K
	Feedwater temperature 288 K
	Feedwater pressure 5 MPa

The maximum amount of water that can be injected in the AC is limited by the saturation of the water. Assuming the complete evaporation of the water, the partial pressure of the vapor in the mixture leaving the AC can be evaluated from the Dalton equation:

$$p'_{3,w} = p_3 \frac{\dot{m}_w/MW_w}{\dot{m}_{a,3}/MW_a + \dot{m}_w/MW_w} \tag{5}$$

where the difference between stagnation and static pressure is neglected because the flow velocity is low. From the partial pressure $p'_{3,w}$ of the water it is possible to evaluate the corresponding saturation temperature T_{sat} as shown in Fig. 3a. From Eq. (5) it appears that $p'_{3,w}$ and T_{sat} are dependent on x_w. The maximum amount of water that can be injected in the AC is given by the saturation condition:

$$T_3 = T_{\text{sat}} \tag{6}$$

This condition corresponds to the point in which the plot of T_3 crosses the plot of T_{sat}. Figure 3a shows that the limit of saturation with the ECO is reached for $x_w = 0.135$.

The air–vapor mixture exiting the AC is heated in the R that is a stationary countercurrent heat exchanger. Unlike Refs. 2 and 5, no water is considered to be injected in the R.

In the ECO the water is preheated by the exhaust gas leaving the R. Before entering the ECO, water is pumped to a pressure sufficient to avoid the vaporization of the water in the heat exchanger. With the assumption that the feed-water pressure is equal to 5 MPa (corresponding to the vaporization temperature of 537 K) and $\Delta T_{\min} = 20$ K, the maximum water temperature at the ECO outlet is $T_{H2} = 517$ K. In Fig. 3b the temperature T_{H2} is plotted as function of x_w. It appears that for x_w higher than 0.13 the heat recovered from the exhaust gas is not sufficient to heat the water up to the temperature of 517 K because the temperature T_9 of the exhaust gas leaving the R is lower than 537 K.

Note that, at the saturation limit, the temperature T_{10} (Fig. 3b) of the exhaust gas convoyed to the stack is about 400 K. Taking into account that the dew point of the exhaust gas is about at $T = 350$ K, it appears, for the nonintercooled RWI cycle and for a pressure ratio of an aeroderivative gas turbine that there is only a little place to

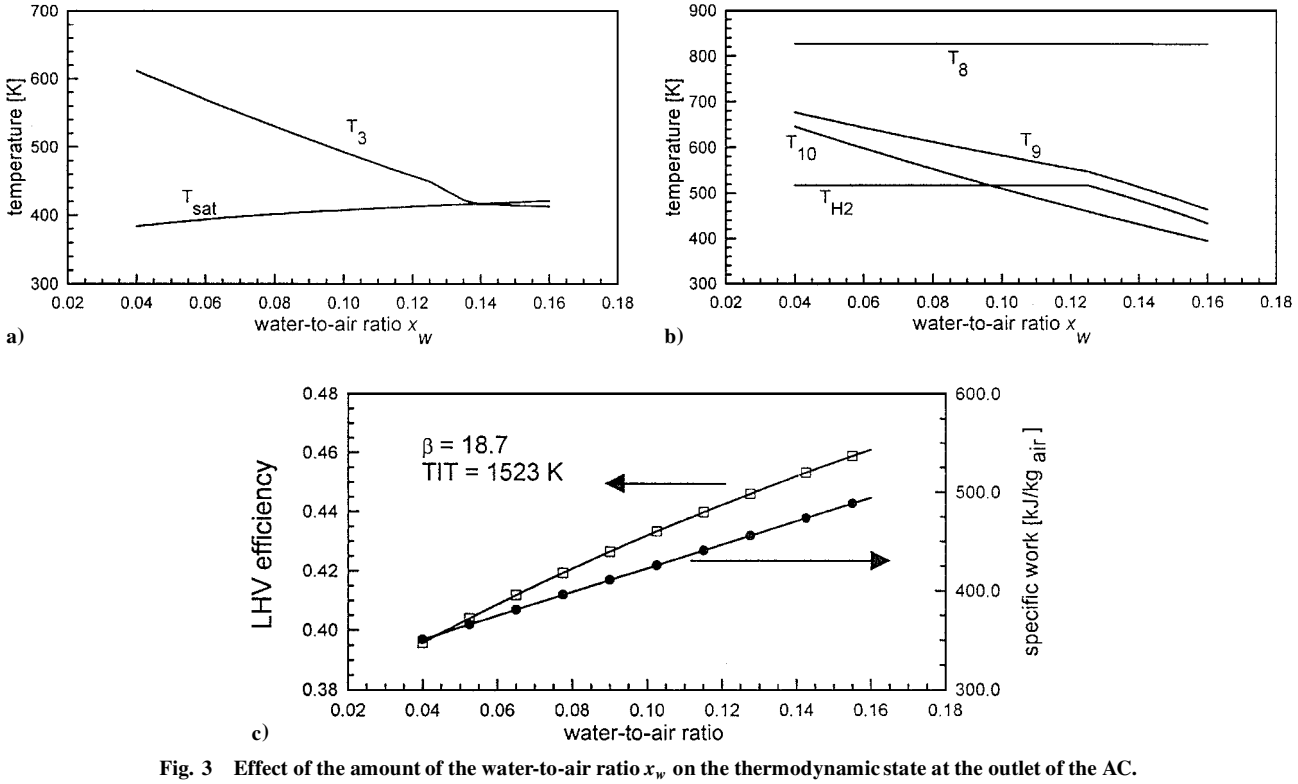

Fig. 3 Effect of the amount of the water-to-air ratio x_w on the thermodynamic state at the outlet of the AC.

increase the exhaust heat recovery with further water injection in the regenerator.

Figure 3c shows the increase of the lower heating value (LHV) efficiency given by water injection in the RWI cycle. It appears that the efficiency can be increased from the basic value of 0.375 of the simple joule cycle aeroderivative gas turbine to the maximum value of 0.45 obtained with the saturation at aftercooler outlet. Figure 3c also shows the increase of the specific work per air mass unit at the compressor inlet. The specific work can be increased from about 346 kJ/kg obtained in the base aeroderivative gas turbine to the maximum value of 480 kJ/kg obtained in the RWI cycle.

C. Effects of the Pressure Ratio

A thermodynamic analysis of the RWI cycle is carried out to outline the effects of the variation of the pressure ratio on LHV efficiency and specific work. Because the efficiency increases with the amount of water injected, for each value of the pressure ratio the amount of water injected needed to reach the saturation is evaluated. Efficiency and specific work are evaluated for pressure ratios ranging from 16 to 22 and for x_w ranging from 0.04 to 0.14. The results are plotted in Fig. 4.

It appears that the maximum efficiency for the RWI cycle is obtained at the saturation limit for any value of the pressure ratio. The best efficiency point ($\eta = 0.455$) is obtained for $\beta = 16$ and $x_w = 0.125$. By the increasing of the pressure ratio, the maximum efficiency is lowered to 0.44 at $\beta = 22$. This result confirms that the RWI cycle may be a useful opportunity for upgrading aeroderivative gas turbines due to the increase of efficiency and power output per mass unit of added water.

D. Effects of the Turbine Inlet Temperature

Figure 5 shows the effects of the TIT variations on efficiency and specific work, considering the saturation limit. It appears that, at any value of pressure ratio and turbine inlet temperature, the increase of the water-to-air ratio provides to increase both the efficiency and the specific work. Moreover, the temperature increase is more effective in raising both efficiency and specific work for $\beta = 20$ than for $\beta = 16$: This is mainly due to the effect of the increase of the amount of cooling air extracted for blade cooling.

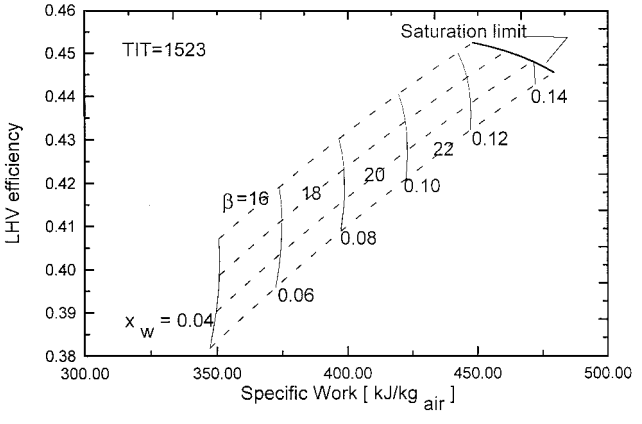

Fig. 4 Effects of the pressure ratio and of the amount of the water injected on the cycle efficiency and the specific work.

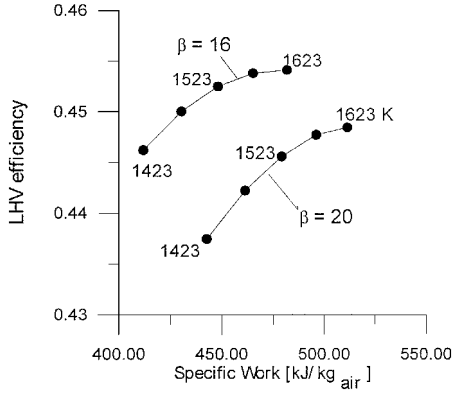

Fig. 5 Effects of the turbine inlet temperature on the efficiency and the specific work.

IV. Performance of the Upgraded Gas Turbine

In the thermodynamic analysis, the pressure ratio, the turbine inlet temperature, the amount of water injected, and other the parameters affecting the air cooled expansion can be assigned by the designer. For predicting the performance of a power plant obtained by upgrading of an existing gas turbine, an off-design analysis of the gas turbine in the upgraded plant configuration is required.

The enhanced gas turbine is supposed to be obtained without modifications of the compressor. For the General Electric Company LM 2500, a rather old characteristic map is available.[10] Because this map shows the design point pressure ratio equal to 18, the map is partially modified to drive the design-point pressure ratio to 18.7. The compressor map used for calculations is shown in Fig. 6.

The characteristic curve of the HPT was not available from the literature. Therefore, the characteristic curve is obtained using the stage-by-stage off-design model described in Appendix A. Figure 7 shows the characteristic curve of the HPT obtained from calculations carried out at various rotational speeds assuming the turbine inlet stagnation values of pressure and temperature to be constant. It appears that at the design point the HPT can be considered choked. The map shows that the mass flow has a very low sensitivity to the speed variation. Figure 7 also shows the cooled turbine efficiency, which is evaluated as

$$\eta_T = P_T \Big/ \sum_j \dot{m}_j c_{pj} T^0_{j,\text{in}} \left[1 - \left(\frac{p^0_{\text{out}}}{p^0_{j,\text{in}}} \right)^{(k_j - 1)/k_j} \right] \tag{7}$$

where the sum is extended to the mainflow and the coolant streams entering in the turbine. The performance of the upgraded gas turbine are predicted considering the operating region of gas generator.[6,8] The off-design analysis is made using the following hypotheses.

1) The characteristics of the HPT blades (diameter, height, heat transfer area on both the gas side and the coolant side) are assumed to be unchanged with respect to the base engine. To increase the throat area in the stator rows where the flow is close to the choking, the modification of the stator blade exit angle is considered.

2) The maximum coolant mass flow is assumed to be limited by the characteristics of the blade channels and obtained from the Eq. (A20) (Appendix A) assuming the value of the characteristic K unchanged.

3) The compressor map is unaffected by the modifications.

4) Heat recovery in the R and in the ECO is evaluated under the same assumptions of the thermodynamic analysis.

The analysis of the performance of the upgraded gas turbine is organized in the following subsections: evaluation of the gas generator operating point, effects of the reduction of the turbine inlet temperature, effects of the variation of the rotational speed, and effects of the reduction of the coolant temperature to decrease the blade temperature.

A. Operating Point of the Upgraded Gas Generator

The analysis of the performance of the gas generator is carried out independently from the characteristics of the power turbine. The working points of the gas generator are determined by the following conditions: 1) mechanical equilibrium of the gas generator shaft (the power produced by the HPT must be equal to the power absorbed by the compressor) and 2) flow compatibility (mass flow, stagnation pressure, and temperature at the HPT inlet must be compatible with the HPT characteristics).

The expected LHV efficiency and power output are evaluated assuming that the polytropic efficiency of the power turbine is equal to 0.9. Three independent parameters have to be assigned to determine any working point of the gas generator in an RWI cycle. In the

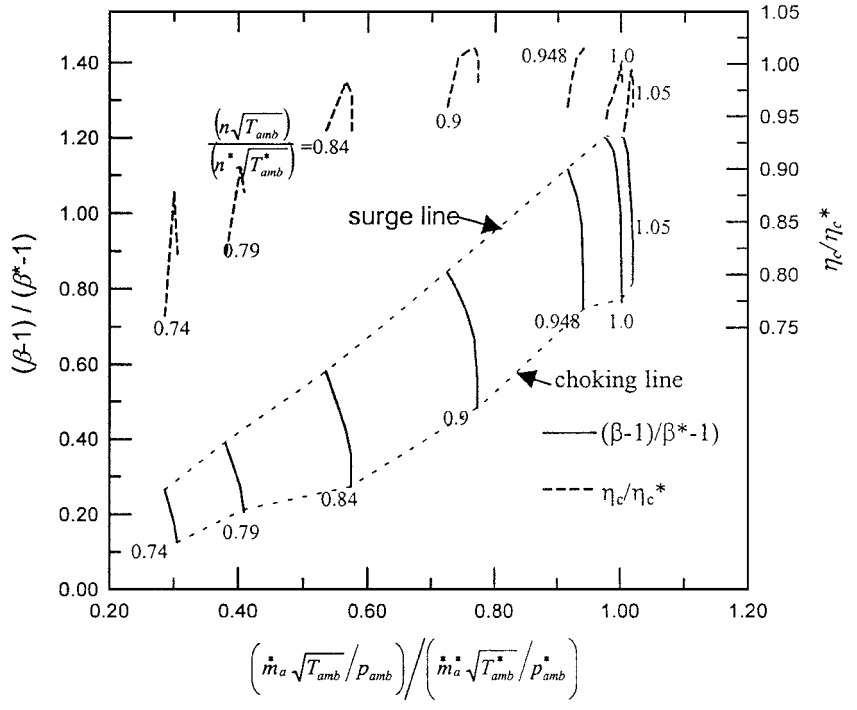

Fig. 6 Characteristic map used (data extracted from Ref. 9).

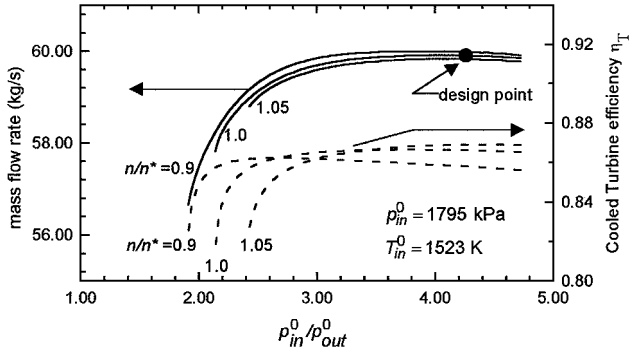

Fig. 7 Estimated characteristic map of the HPT.

following analysis they are the shaft rotational speed, the turbine inlet temperature, and the water-to-air ratio x_w.

First the analysis is carried out at the rotational speed of 9655 rpm, which is the nominal speed of the gas generator. The compressor characteristic map (Fig. 6) shows that, at this speed, the air mass flow is almost constant and independent from the pressure ratio (at least not close to the surge limit). The water mass flow $\dot{m}_w$ added to the flow modifies the matching conditions of the compressor with the HPT because of the increased mass flow at the HPT inlet. In fact, because $\dot{m}_a$ is about constant, neglecting the variations of the cooling air and fuel mass flow, $\dot{m}_g$ can also be considered constant. Therefore, referring to Eq. (2), the total mass flow $\dot{m}$ at the HPT inlet is increased the same quantity as the water injected.

Because the HPT at the design point is choked (Fig. 7), the mass flow parameter of the HPT

$$\Gamma = \dot{m}\sqrt{T^0_{\text{in}}}\Big/ p^0_{\text{in}} \tag{8}$$

is equal to its maximum value. The increase of the mass flow produced by water injection needs to be compensated by the increase of the inlet pressure p^0_{in} or by the decrease of the turbine inlet temperature T^0_{in}. Analogously to the steam-injected gas turbines,[16] it is possible to increase pressure ratio reducing the surge margin with respect to the value adopted in the base aeroengine. The surge margin can be assumed as

$$S = (\beta_S - \beta)/(\beta - 1) \tag{9}$$

where β is the pressure ratio of the compressor working point and β_s is the pressure ratio on the surge line at the same compressor rotational speed of the considered working point. In the base aeroderivative gas turbine at the design point ($n = 9655$ rpm, $n = 18.7$) the surge margin is about 20%. By consideration of a reduction of the surge margin to 15%, the limiting value of the pressure ratio at 9655 rpm is then placed at 19.6.

Because of the pressure losses in the aftercooler (3%) and in the regenerative heat exchanger (2%), the increase of the pressure ratio from 18.7 to 19.6 is sufficient only to compensate for the pressure loss in the additional devices, but no increment is produced for the stagnation pressure at the HPT inlet.

The amount of water that can be injected without modification of the HPT is affected by the compressor map. Therefore, the quantitative results that will be provided in the following section have to be considered in strict relationship with the assumed compressor map. With the map of the General Electric Company LM 2500 considered here, the air mass flow at the design rotational speed is about constant. Therefore, to avoid an unacceptable reduction of the turbine inlet temperature, it is necessary to modify the HPT to accommodate the larger mass flow. Note that the operating points of the upgraded gas turbine are affected by the compressor characteristic map. In Ref. 8, for example, the authors, using a generalized map, found that a limited amount of water was allowed to be injected.

The turbine flow parameter can be increased by increasing the effective throat area in the stator rows of one or both the stages where the turbine is close to being choked. Variation of the area can be accomplished by modifying the stator exit blade angle. As a first case, a limited amount of water injected ($x_w = 0.05$) is considered. To evaluate the effect of opening the nozzle passage, the first-stage stator blade exit angle α_2 is reduced. Figure 8 shows the effects produced by such a variation of the first-stage nozzle passage, provided that the turbine inlet temperature is constant. It appears that the decrease of α_2 leads to the reduction of the pressure ratio: the pressure ratio corresponding to the surge margin (19.7) is obtained with $\Delta\alpha_2 = -2$ deg.

A negative incidence angle on the first-stage rotor blade is caused by the variation of α_2, while the incidence on the blades of the other rows is about zero. For $\Delta\alpha_2 = -2$ deg, the incidence angle at the inlet of the first-stage rotor is about $\Delta\theta = -10$ deg, which is mainly due to the decrease of $M_{2,\text{st}}$ with respect to the value obtained in the base engine. In fact, lowering the compressor pressure ratio the work per

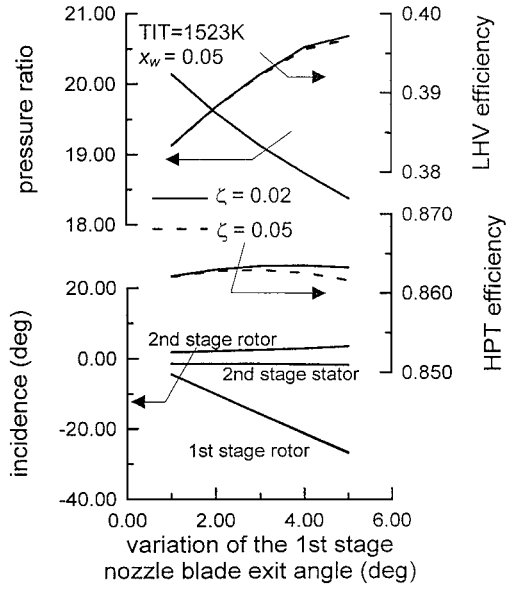

Fig. 8 Effects of opening the first-stage nozzle vane passage.

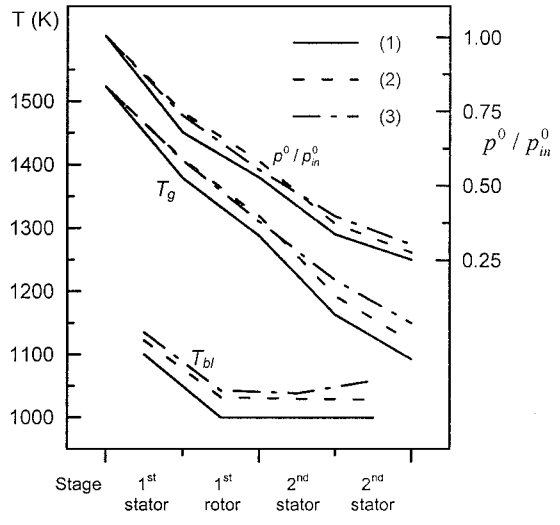

Fig. 9 Temperature and pressure distribution in the HPT. 1) Base engine, 2) RWI cycle with x_w = 0.05 after opening first-stage stator vane passage, 3) RWI cycle with x_w = 0.1 after opening first- and second-stage stator vane passage.

mass unit produced by the HPT is decreased, as required by the mechanical equilibrium of the gas generator shaft. The row efficiency is related to the incidence angle by Eq. (A17) (Appendix A). Two values of the loss coefficient ζ are considered: $\zeta = 0.02$ and 0.05. It appears that, until $|\Delta\theta|$ is lower than 20 deg, the turbine efficiency decrease is lower than 1% and has a little effect on the plant efficiency.

For $x_w = 0.1$, the throat area of both the stages has to be increased. After a trial and error procedure, a reduction of 4 deg of the stator exit angle α_2 (for which the throat area is increased of about 20%) has been found to be necessary to match the compressor and HPT at the desired working point. In this case β resulted about 19. The maximum incidence angle is 15 deg at the second-stage rotor inlet.

To increase x_w to above 0.1, the rotor blades also need to be modified to avoid excessive incidence angles.

To analyze the effects of the increased mass flow on the blade temperature, the gas temperature and the blade temperature in the modified HPT are shown in Fig. 9. In the stator rows, the gas temperature is equal to the absolute (stator relative) stagnation temperature. In the rotor rows, the rotor relative stagnation temperature is considered (Appendix A). Figure 9 shows that the combined effect of the lower gas temperature drop and of the increased mass flow causes the blade temperature to increase above the blade temperature of the base engine. In the case of $x_w = 0.05$, the temperature increase is about 30°C on all of the rows. In the case of $x_w = 0.1$, the maximum blade temperature increase is equal to 70°C and is obtained for the last rotor row.

B. Effects of the TIT Reduction

To decrease the blade temperature, it is possible to decrease the TIT. In Fig. 10 the effects of the TIT reduction are analyzed. It appears that the reduction of the blade temperature obtained by decreasing the turbine inlet temperature is very small. The decrease of the blade temperature for the second stage (not shown) is a little faster than for the first stage. The HPT efficiency is not affected by the reduction of the TIT.

To match the blade temperature limits the turbine inlet temperature needs to be lowered to 1460 K for $x_w = 0.05$ and to 1420 K for $x_w = 0.1$. By the decreasing of the TIT, the plant efficiency and power output are lowered, notwithstanding the decrease of the pressure ratio. The blade limits are shown in Fig. 10 by horizontal lines. It appears that for $x_w = 0.1$ the maximum efficiency 0.40 is obtained with TIT = 1420 K. The plant efficiency is, therefore, 4% lower than the value obtained in the thermodynamic analysis for $x_w = 0.1$, $\beta = 18.7$, and TIT = 1523 K.

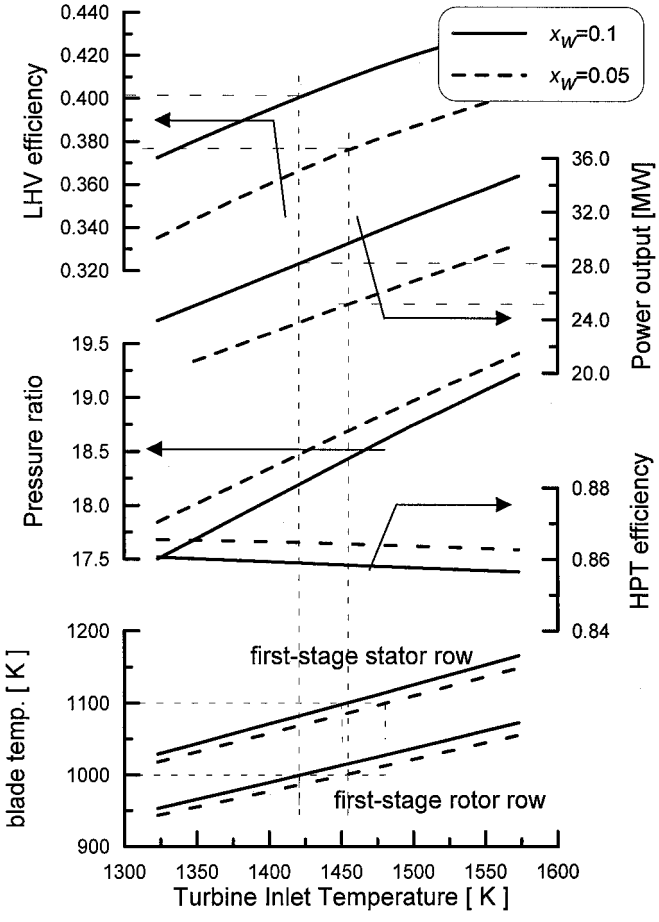

Fig. 10 Variation of the gas generator working conditions with water injection and modified HPT stator vane passages at constant speed, n = 9655 rpm.

C. Gas Generator Operating Region

The most suitable working conditions, at various gas generator speeds, can be found with the aid of the analysis of the whole gas generator operating region. Figure 11 shows the limits of the gas generator operating region and the contours of the expected plant efficiency and power obtained for $x_w = 0.1$. The boundaries of the region are given by the compressor surge limit, by the compressor choking limit, by the maximum rotational speed, and finally by the

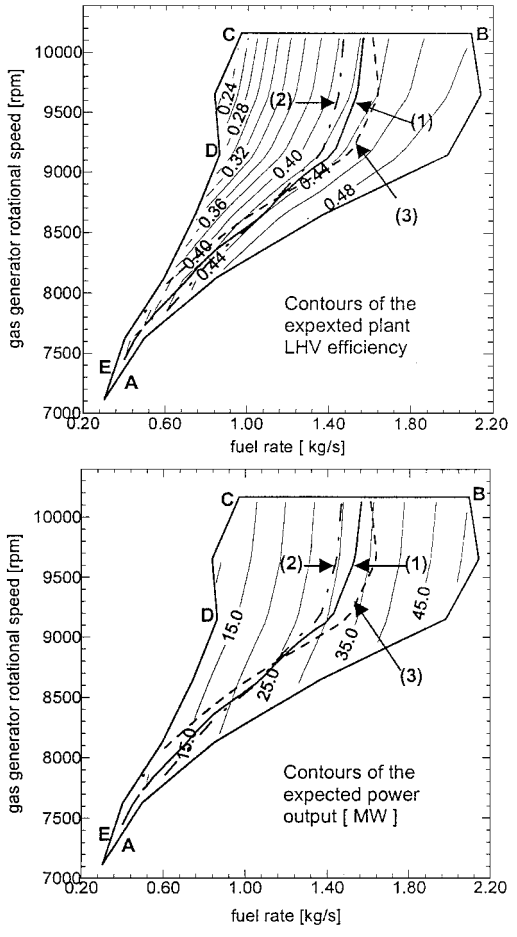

A-B : compressor surge limit
B-C: compressor maximum rotational speed
C-D: limit given by the compressor choking
D-E: limit given by the saturation at the aftercooler outlet
(1) TIT=1523 K;
(2) 1st stage stator blade temp=1100 K
(3) Surge margin=15%

Fig. 11 Contours of the expected efficiency and power output within the gas generator domain of the RWI cycle gas turbine with x_w = 0.1 after opening the vane passages.

limit given by the saturation at the aftercooler outlet. Figure 11 also shows the limits of the maximum allowable temperatures on the first-stage nozzle as well as the curve of surge margin. For the sake of clarity, the limit curves of the blade temperature concerning the other rows are not reported inasmuch as they are close to the other blade temperature limit.

Figure 11 shows that the maximum LHV efficiency within the limits given by the blade temperature is obtained at rotational speed lower than the nominal one. This is mainly due to the favorable effects of the reduction of the pressure ratio and the increase of the turbine inlet temperature. A little increase of the compressor isentropic efficiency, shown in the compressor map, contributes the improvement of the overall LHV efficiency. The drawback is that the power output is lowered due to the decrease of the air mass flow. At 9172 rpm, the maximum expected efficiency is 0.42, and the corresponding power output is 27 MW.

D. Performance of the Upgraded Gas Turbine with Lower Coolant Temperature

To increase the cooling efficiency required to match the modified working conditions of the HPT, it is possible either to design a new blade cooling system or to lower the coolant temperature, taking advantage of the available cold water, without modifying the blade characteristics. The latter choice is considered in this work. In any case, the coolant can no longer be extracted from the plenum outside the combustion chamber because the temperature of the air leaving the R is much higher than the temperature of the air leaving the compressor in the base engine. The lower coolant temperature allows more heat per coolant mass unit to be removed from the blade. Moreover, the coolant specific volume is lowered. This allows the increase of the coolant mass flow as predicted by Eq. (A20) in Appendix A.

Two alternative solutions may be analyzed for lowering the temperature of the coolant entering the blade channels. The first is obtained by means of a water–air heat exchanger in which the coolant temperature is reduced; the second is obtained by using a fraction of the water–air mixture leaving the AC as cooling air. The former solution will be analyzed here. The second solution is more effective for a thermodynamic point of view because the air–water mixture has a larger specific heat coefficient.[8] However, this solution requires the modification of the compressor to vary the amount of cooling air and the point of extraction. This may affect the compressor map and is excluded from the hypotheses of the analysis carried out here.

The heat exchanger is introduced in the coolant circuit from the compressor to the blade row. The coolant temperature should be decreased as much as required to keep the blade temperature at the prescribed value. Excessive coolant temperature reduction should be avoided because it causes a decrease of the overall efficiency.

The effects of the coolant temperature decrease on the blade heat balance are examined in Fig. 12 for the stator rows of the first and second HPT stages. The effects on the blade temperature, coolant mass flow, internal heat transfer efficiency ε, and cooling system effectiveness Φ are plotted as functions of the coolant temperature decrease $\Delta T_{\rm cl}$. In Fig. 12 the blade temperature is nondimensionalized by the prescribed $T_b^* = 1100$ K, and the coolant mass flow is nondimensionalized by the value $\dot{m}_{\rm cl}^*$ at the design point.

It appears that the effects of the coolant temperature reduction on the internal cooling efficiency are negligible. The increase of the heat flux is, therefore, due to the lower coolant temperature at the blade inlet and to the increased coolant mass flow [see Eq. (A12), Appendix A]. For the first-stage row, the prescribed blade temperature is obtained with about $\Delta T_{\rm cl} = 100$ K. For the second stage, which is characterized by a lower cooling system effectiveness ($\Phi = 0.25$),

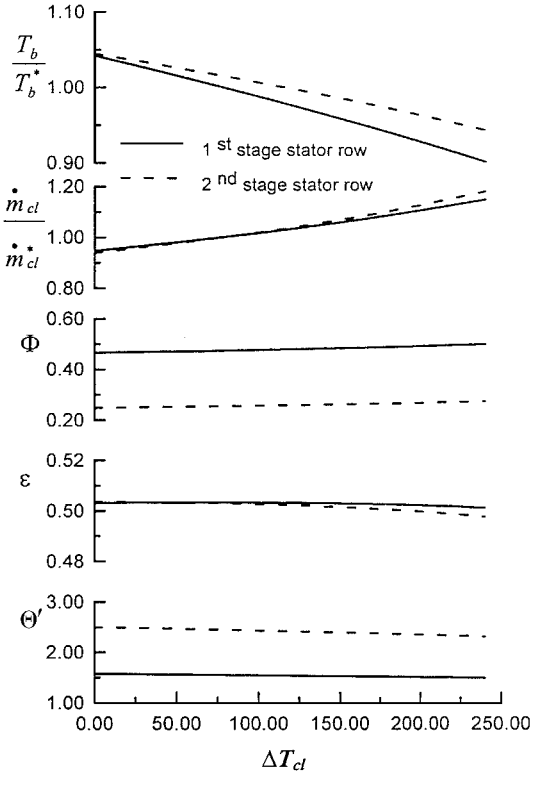

Fig. 12 Variation of the main blade cooling parameters with the reduction of the coolant temperature; TIT = 1523 K, x_w = 0.1.

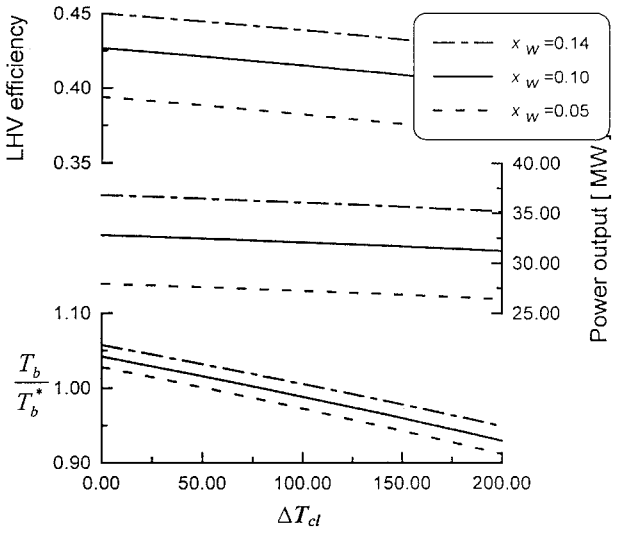

Fig. 13 Performance of the RWI cycle aeroderivative gas turbine with the reduction of the coolant temperature; TIT = 1523 K. T_b is referred to the first stator row.

the decrease of the coolant temperature required to match the prescribed blade temperature is about equal to 200 K. In this case, the possibility of improving the blade cooling effectiveness should be considered to decrease the coolant mass flow and to reduce $\Delta T_{\rm cl}$, also providing a better overall efficiency.

The coolant temperature reduction suggests the possibility of increasing the turbine inlet temperature to increase the efficiency. A more detailed model of the blade cooling system may be useful in this case to investigate blade temperature that may be locally excessively high. The effects of the coolant temperature reduction on the plant performance are analyzed in Fig. 13 for three values of the water-to-air ratio. The increase of ΔT_{cl} causes a little decrease of LHV efficiency and power output. The maximum efficiency point, obtained for $X_w = 0.14$ and $\Delta T_{cl} = 120$ K, is close to 44%.

V. Conclusions

A methodology to analyze the performance of an evaporative cycle power plant obtained upgrading an aeroderivative gas turbine has been presented. The methodology is based on a modular model able to analyze the off-design behavior of a generic configuration of gas-turbine power plant.

The main features of the proposed method are as follows.

1) The capability to take into account the variations the thermodynamic properties of the working fluids produced by water injection is introduced.

2) The off design turbine blade cooling system effectiveness and blade temperatures, as result from variation of the cooling air flow rate and thermodynamic conditions, are estimated.

3) Mass flow rate variations in the secondary air cooling system are considered. The methodology has been applied to the design of a power plant based on the RWI cycle. The thermodynamic analysis has shown that the a RWI cycle gas turbine obtained from a typical aeroengine may offer plant efficiency up to 44% and expected power output is 30% larger than the power output that can be obtained in the simple Joule cycle gas turbine obtained from the same aeroengine.

The modifications of the gas generator required to realize the RWI cycle gas turbine are then analyzed. Modifications of the core engine considered do not affect the multistage compressor. It is shown that the modification of the HPT vanes is needed to accommodate the larger mass flow rate produced by water injection. Up to $x_w = 0.1$, the modifications may be limited to the stator blades; in this case a low reduction of the efficiency caused by the off-design flow incidence is observed. For further increase of the water mass flow, the rotor inlet and exit blade angles also should be modified.

The performance of the cooling system is analyzed. The increase of the mass flow drives the blade temperature to levels that may be not compatible with the material. To meet the blade temperature limit, the turbine inlet temperature should be reduced. The best efficiency point in this plant configuration has been analyzed.

Moreover the reduction of the coolant temperature has been examined as alternative solution. This solution allows the reduction of the blade temperature within the prescribed limit without a complete new design of the blade cooling system.

The procedure proposed for the analysis of the aeroengine to realize the RWI cycle gas turbine may be also applied to other mixed gas–steam cycles.

Appendix A: Mathematical Model of the Air-Cooled Turbine

A. Numerical Solution Method

Off-design performances are predicted by means of a model entirely of the authors' creation able to handle a power plant at on-design and off-design conditions. The gas turbine is described by a set of nonlinear algebraic equations that is solved through a methodology based on the Newton–Raphson method, with the evaluation of the Jacobian matrix by finite differences. To avoid the tendency of the Newton–Raphson method to wander off if the initial guess is not close to the root, a lower and an upper bound are assigned to each variable: If the solution for one variable is addressed outside the limits, the guess is forced to be placed on the bound closer to the value obtained from calculation. In a few cases, a globally convergent method based on a line search strategy is found to be necessary.

B. On-Design Turbine Stage Model

The turbine on-design performance is evaluated by means of a stage-by-stage analysis of the expansion. The same procedure has been used for the thermodynamic analysis of the RWI cycle.

The model of the expansion in a cooled turbine stage is similar to the model proposed by El-Masri[13] and shown in Fig. A1. The enthalpic drop in the stage is divided in the following steps: (A–C) mixing of the hot gas with the stator row cooling air, (C–D) adiabatic expansion with work production, and (D–F) mixing of the hot gas with the rotor row cooling air.

The mixing process A–C is schematically divided into two steps: a mixing process (A–B) without loss of stagnation pressure, where the mainstream specific enthalpy is reduced by the mixing with the stator cooling flow, and a pressure loss (B–C) due to the momentum loss of the mainstream flow. The same scheme is used for the mixing process with the rotor cooling flow (D–F).

To evaluate the adiabatic expansion C–D, a one-dimensional model is assumed for the velocity diagram, referred to the middle chord of the blade (Fig. A2). For simplicity, the axial velocity and the mean diameter are assumed to be constant in the stage and

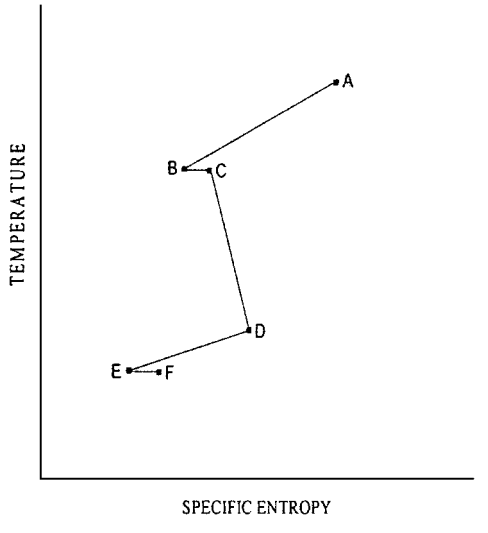

Fig. A1 Thermodynamic states of the expansion model in an air-cooled turbine stage.

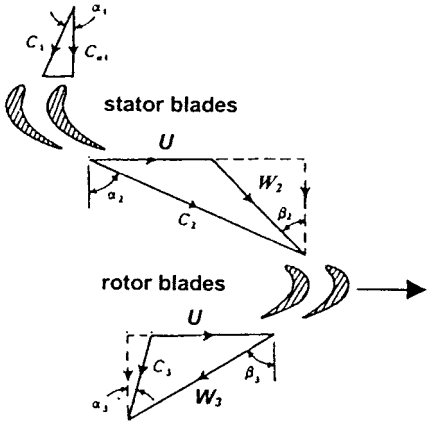

Fig. A2 Velocity triangles in the axial flow turbine stage.

the rotor-exit swirl angle (α_3) is zero. The velocity triangles are evaluated from the assigned values of the dimensionless coefficients,

$$\phi = C_{a2}/U, \qquad \Psi = w_t/U^2 \tag{A1}$$

where w_t is the work per mass unit produced in the stage. The flow is assumed to be subsonic.

The stagnation temperature drop from state A to state B is given by the steady flow energy equation,

$$T_B^0 = (1/\dot{m}_B \cdot c_{p,\mathrm{cl}})\left(\dot{m}_A \cdot c_{p,g} \cdot T_A^0 + \dot{m}_{\mathrm{cl,st}} \cdot c_{p,\mathrm{cl}} \cdot T_{\mathrm{cl,st}}^0\right) \tag{A2}$$

The stagnation pressure loss due to the mixing of the mainstream with the coolant is evaluated from

$$p_C^0 = p_B^0 \cdot \left[1 - (\dot{m}_{\mathrm{cl,st}}/\dot{m}_B)(1 - Y_{\mathrm{st}}) \cdot k \cdot M_{2,\mathrm{st}}^2\right] \tag{A3}$$

where Y_{st} is a momentum-loss parameter[7,13] and $M_{2,\mathrm{st}}$ is the absolute Mach number at the stator exit. The value of $M_{2,\mathrm{st}}$ is obtained from the absolute velocity c_2 and the energy equation applied to the stator row. The stagnation temperature and pressure at the end of the adiabatic expansion C–D are given by

$$T_D^0 = T_C^0 - w_t/c_{p,g} \tag{A4}$$

$$p_D^0 = p_C^0 \cdot \left[1 - (1/\eta_t)\left(1 - T_D^0/T_C^0\right)\right]^{k/(k-1)} \tag{A5}$$

where η_t is the total-to-total stage adiabatic efficiency. The thermodynamic conditions in points E and F are evaluated similarly to points B and C, considering the rotor relative Mach number $M_{3,\mathrm{rot}}$ for the evaluation of the momentum losses in the rotor row.

The estimation of the blade temperature is made under the hypothesis that the blade is at uniform temperature T_b.[7,13] As it is common in aeroderivative gas turbines, the blade is considered cooled by internal cooling and film cooling. With reference to the adiabatic wall temperature[17,18] T_{ad}, the heat flux balance across the blade wall gives

$$h_e A_e (T_{\mathrm{ad}} - T_b) = \dot{m}_{\mathrm{cl}} c_{p,\mathrm{cl}} \Delta T_{\mathrm{cl}} \tag{A6}$$

where h_e is the heat transfer coefficient on the gas side of the blade, A_e is the external wall area of the blade, and $\Delta T_{\mathrm{cl}} = (T_{\mathrm{cl},2} - T_{\mathrm{cl},1})$ is the coolant temperature rise through the internal cooling circuits. The coolant temperature rise depends on the internal heat transfer efficiency ε and from temperature $T_{\mathrm{cl},1}$ at which the coolant is supplied,

$$\varepsilon = \Delta T_{\mathrm{cl}}/(T_b - T_{\mathrm{cl},1}) \tag{A7}$$

Under the hypothesis that the blade temperature is uniform, the internal heat transfer efficiency is given by

$$\varepsilon = 1 - \exp[(-h_i A_i)/(\dot{m}_{\mathrm{cl}} c_{p,\mathrm{cl}})] \tag{A8}$$

where h_i is the internal heat transfer coefficient and A_i is the internal wall area of the blade. The product $h_e A_e$ is evaluated from the Stanton number St_e of the hot stream and from the ratio of the wall area A_e to the gas flow path cross-sectional area A_g at the row inlet,[7,17]

$$St_e = \frac{h_e}{(\dot{m}_g/A_g) \cdot c_{p,g}} = \frac{h_e A_e}{\dot{m}_g \cdot c_{p,g}} \cdot \frac{A_g}{A_e} \tag{A9}$$

The adiabatic wall temperature is estimated from the adiabatic film cooling effectiveness

$$\eta_{f\,\mathrm{ad}} = \frac{T_{\mathrm{ad}} - T}{T_{\mathrm{cl},2} - T_g} \tag{A10}$$

and the dimensionless parameter

$$\Theta = \frac{T_{\mathrm{cl},2} - T_g}{T_b - T_g} \tag{A11}$$

The gas temperature T_g is assumed equal to the absolute stagnation temperature for the stator rows and equal to the rotor relative stagnation temperature for the rotor rows.

The heat flux across the blade can then be written, considering Eqs. (A7), (A10), and (A11),

$$h_e A_e (T_g - T_b)(1 - \Theta\eta_{\mathrm{ad}}) = \dot{m}_{\mathrm{cl}} c_{p,\mathrm{cl}} \varepsilon (T_b - T_{\mathrm{cl},1}) \tag{A12}$$

For a considered maximum allowable blade temperature T_b, Eq. (A11) allows evaluation of the coolant mass flow per each row, assuming the values of St_e, ε, and η_{ad}.

C. Off-Design Stage Performance

The off-design expansion is modeled, as for the on-design analysis, by means of the scheme shown in Fig. A1. The adiabatic expansion C–D is determined by the off-design stage velocity diagram and the efficiency of the stator and the rotor rows. The stage velocity triangle is evaluated at the pitch line from constructive data about blade angles and cross-sectional area of the stage. By the assuming that the flow is subsonic and that the axial flow velocity is constant in the stage, the stage aerodynamic load is related to the flow coefficient by

$$\Psi = \phi(\tan\alpha_2 - \tan\beta_3) - 1 \tag{A13}$$

assuming the flow angles are equal to the blade angles.

The flow coefficient ϕ is related to the gas mass flow by the compatibility equation evaluated at the stator exit:

$$\dot{m}_g = A_g \rho_g \phi U \tag{A14}$$

The thermodynamic state at the stator row (rotor) exit is obtained from the row efficiency,

$$\eta_{\mathrm{row}} = \frac{V_{\mathrm{out}}^2/2}{V_{\mathrm{out,is}}^2/2} \tag{A15}$$

where V_{out} is the actual absolute (relative) velocity $c_2(w_3)$ and $V_{\mathrm{out,is}}$ is the velocity for the isentropic expansion. The row efficiency is estimated from the flow incidence angle $\Delta\theta$ at the row inlet, given by

$$\Delta\theta = \theta_i - \theta_i^* \tag{A16}$$

where θ_i and θ_i^* are the stator (rotor) inlet flow angle $\alpha_1(\beta_2)$ at the off-design point in the HPT and the blade geometric angle α_1^* (β_2^*), respectively.

The relation proposed by Kroon and Tobiasz[19] is used:

$$\eta_{\mathrm{row}} = \eta_{0,\mathrm{row}} - \zeta \tan^2 \Delta\theta \tag{A17}$$

where $\eta_{0,\mathrm{row}}$ is the value of η_{row} for zero incidence and ζ is a coefficient indicating the sensitivity of the blading to the variations in the angle of incidence.

The estimation of the blade temperature is made from Eq. (A12) taking into account the variation of all of the parameters that appear therein. At off-design conditions the internal cooling efficiency ε is evaluated from the variations of the ratio $h_i/(\dot{m}_{\mathrm{cl}} \cdot c_{p,\mathrm{cl}})$ that is proportional to the internal Stanton number. By assuming that the internal convection cooling follows the Colburns formula (see Ref. 17)

$$St_i \propto Re^{-0.2} \cdot Pr^{-\frac{2}{3}} \tag{A18}$$

it is possible to obtain the corresponding values at off-design conditions:

$$St_i \propto (\dot{m}_{\mathrm{cl}}/\mu_{\mathrm{cl}})^{-0.2} \cdot (\mu_{\mathrm{cl}} \cdot c_{p,\mathrm{cl}})^{-\frac{2}{3}} \tag{A19}$$

The gas side Stanton number and the adiabatic film cooling coefficient are assumed to be constant.

For the evaluation of the coolant mass flow, it should be considered that the cooling air flow path in a compressor–turbine assembly is rather complicated because it is composed of a network of restrictions, cavities, and blade holes for film cooling. Lacking detailed information about these elements, the coolant flow rate can be predicted, in accordance with experimental results of McGreehan and Schotsch,[20] through the orifice equation

$$\dot{m}_{cl}\sqrt{T_{in}}\Big/ p_{in} = K \cdot \sqrt{1 - p'_{out}/ p_{in}} \qquad \text{(A20)}$$

where K accounts for the discharge coefficient and the area of the orifice; p_{in} and T_{in} are, the stagnation pressure and temperature at the orifice inlet, respectively; and p'_{out} is the outlet static pressure. The coefficient K is evaluated from value of the cooling air flow rate at the gas-turbine design point.

Appendix B: Results of the Design Process for the Base Aeroderivative Gas Turbine

For the compressor, the pressure ratio $\beta = 18.7$. The power absorbed by the compressor was 29.1 *MW*. The compressor isentropic efficiency was 0.870. The shaft power was equal to 23.25 *MW* and specific work was 346.0 kJ/kg. The LHV efficiency was 37.6%. The electric power at the generator terminals was 22.79 *MW*. The specific fuel consumption was 9771 kJ/kWh. The results of the design process are summarized in Table B1.

For the HPT performance, the cooled turbine efficiency was 0.867. The first-stage cooled efficiency was 0.844, and the second-stage cooled efficiency was 0.880. The HPT characteristics are summarized in Tables B2 and B3.

Table B1 Design process results

Cycle state points	Stagnation pressure, kPa	Stagnation temperature, K		Mass flow, %
		Absolute	Rotor relative	
Compressor inlet	100.0	288.0	——	100.0
Compressor discharge	1870.0	703.0	——	87.0
Comb. discharge	1795.2	1523.0	——	88.8
HPT inlet rotor 1	1159.4	1492.0	1375.8	92.3
HPT outlet rotor 1	918.4	1290.0	——	96.6
HPT inlet rotor 2	546.2	1267.0	1147.1	100.0
HPT outlet rotor 2	415.4	1078.8	——	101.8
Power turbine outlet	105.5	795.1	——	101.8

Table B2 HPT characteristics at the mean diameter

Location	Absolute		Rotor relative		Mean diam, m	Hub-to-tip ratio
	Angle, deg	Mach number	Angle, deg	Mach number		
Stage 1						
Rotor inlet	71.6	0.85	45.0	0.38	0.765	0.88
Rotor exit	0	0.27	63.4	0.61	0.765	1.13
Stage 2						
Rotor inlet	71.6	0.93	45.0	0.42	0.765	1.26
Rotor exit	0	0.30	63.4	0.67	0.765	1.31

Table B3 HPT cooling system characteristics

Location	Blade temp., K	Cooling effectiveness	Extraction pressure, kPa	Extraction temp., K	Mass flow, %
Stator 1	1100	0.52	1870.0	703.0	3.4
Rotor 1	1000	0.57	1870.0	703.0	4.3
Stator 2	1000	0.43	1193.8	616.0	3.4
Rotor 2	1000	0.28	1193.8	616.0	1.8

Acknowledgment

The present work has been supported by Ministero dell' Universita' e della Ricerca Scientifica e Tecnologica (MURST), Italy.

References

[1]Gasparovich, N., and Hellemans, J. G., "Gas Turbines with Heat Exchanger and Water Injection in the Compressed Air," *Proceedings of the Institution of Mechanical Engineers*, Vol. 66, 1971, pp. 953–961.

[2]El-Masri, M. A., "A Modified, High-Efficiency, Recuperated Gas Turbine Cycle," *Journal of Engineering for Gas Turbines and Power*, Vol. 110, April 1988, pp. 233–242.

[3]Annerwall, K., and Svedberg, G., "A Study on Modified Gas Turbine Systems with Steam Injection or Evaporative Regeneration," *ASME Cogen-Turbo*, IGTI-Vol. 6, American Society of Mechanical Engineers, Fairfield, NJ, 1991, pp. 1–7.

[4]Chiesa, P., Lozza, G., Macchi, E., and Consonni, S., "An Assessment of the Thermodynamic Performance of Mixed Gas-Steam Cycles: Part B—Water Injected and HAT Cycles," *Journal of Engineering for Gas Turbines and Power*, Vol. 117, April 1995, pp. 409–508.

[5]Horlock, J. H., "The Evaporative Gas Turbine [EGT] Cycle," American Society of Mechanical Engineers, Paper 97-GT-408, June 1997.

[6]Camporeale, S., and Fortunato, B., "Design and Off-Design Performance of Advanced Mixed Gas–Steam Cycle Power Plants," *Proceedings of 31st International Energy Conversion Engineering Conference*, Institute of Electrical and Electronics Engineers, Piscataway, NJ, Aug. 1996, pp. 695–701.

[7]Bolland, O., and Stadaas, J. F., "Comparative Evaluation of Combined Cycles and Gas Turbine Systems with Water Injection, Steam Injection, and Recuperation," *Journal of Engineering for Gas Turbines and Power*, Vol. 117, Jan. 1995, pp. 138–145.

[8]Camporeale, S., and Fortunato, B., "Performance of a Mixed Gas-Steam Cycle Power Plant Obtained Upgrading an Aeroderivative Gas Turbine," *Proceedings of the 1997 Florence World Energy Symposium*, SG Editoriale, Padova, Italy, Aug. 1997, pp. 365–376.

[9]Tuccillo, R., and Bozza, F., "An Integrated Study of Advanced Cycles and Component Operation in Gas Turbine Power Plants," *Proceedings of the 1994 Florence World Energy Research Symposium*, SG Editoriale, Padova, Italy, July 1994, pp. 381–394.

[10]Spector, R. B., and Miller, A. A., "GE LM 2500 Aircraft-Derivative Gas Turbine System," General Electric Co. Rept. GER 3431, 1983, pp. 1–20.

[11]"Industrial Engine Performance- Natural Gas Fuel," General Electric Co. Rept. URL: http: www.ge.com, Sept. 1997.

[12]Muir, D. E., Saravannamuttoo, H. I. H., and Marshall, D. J., "Health Monitoring of Variable Geometry Gas Turbine for the Canadian Navy," *Journal of Engineering for Gas Turbines and Power*, Vol. 111, April 1989, pp. 244–250.

[13]El-Masri, M. A., "GASCAN-An Interactive Code for Thermal Analysis of Gas Turbine Systems," *Journal of Engineering for Gas Turbines and Power*, Vol. 110, April 1988, pp. 201–209.

[14]Heywood, J. B., *Internal Combustion Engine Fundamentals*, McGraw–Hill, New York, 1988, chap. 4, p. 130.

[15]Casalini, F., and Fortunato, B., "Calcolo automatico del ciclo Rankine," Atti dell'Istituto di Macchine, Univ. di Bari, Bari, Italy, 1984, pp. 1–10.

[16]Rice, I. G., "Steam-Injected Gas Turbine Analysis: Steam Rates," *Journal of Engineering for Gas Turbines and Power*, Vol. 117, April 1995, pp. 347–353.

[17]Chiesa, P., Lozza, G., and Consonni, S., "Gas/Steam Cycles with Open-Circuit Steam Cooling of Gas Turbine Blades," *Proceedings of Florence World Energy Research Symposium*, edited by S. S. Stecco, Univ. of Florence, Italy, 1992, pp. 303–323.

[18]Benvenuti, E., Bettocchi, R., Cantore, G., Negri di Montenegro, and Spina, P. R., "Gas Turbine Cycle Modelling Oriented to Component Performance Evaluation from Limited Design Test Data," *ASME Cogen Turbo'93*, IGTI-Vol. 8, American Society of Mechanical Engineers, Fairfield, NJ, 1993, pp. 327–337.

[19]Kroon, R. P., and Tobiasz, H. J., "Off-Design Performance of Multistage Turbines," *Journal of Engineering for Power*, Vol. 93, Series A, No. 1, 1971, pp. 21–26.

[20]McGreehan, W. F., and Schotsch, M. J., "Flow Characteristics of Long Orifices With Rotation and Corner Radiusing," *Journal of Turbomachinery*, Vol. 110, April 1988, pp. 213–217.